Draft version January 3, 2019
Preprint typeset using LaTeX style emulateapj v. 12/16/11

SDSS-IV MANGA: THE ROLES OF AGNS AND DYNAMICAL PROCESSES IN STAR FORMATION QUENCHING IN NEARBY DISK GALAXIES

Kexin Guo
Kavli Institute for Astronomy and Astrophysics, Peking University, 5 Yiheyuan Road, Haidian District, Beijing 100871, P.R.China and International Centre for Radio Astronomy Research (ICRAR), University of Western Australia, Crawley, WA 6009, Australia

Yingjie Peng
Kavli Institute for Astronomy and Astrophysics, Peking University, 5 Yiheyuan Road, Haidian District, Beijing 100871, P.R.China

Li Shao
Kavli Institute for Astronomy and Astrophysics, Peking University, 5 Yiheyuan Road, Haidian District, Beijing 100871, P.R.China

Hai Fu
Department of Physics and Astronomy, University of Iowa, Van Allen Hall, Iowa City, IA 52242, USA

Barbara Catinella
International Centre for Radio Astronomy Research (ICRAR), University of Western Australia, Crawley, WA 6009, Australia and ARC Centre of Excellence for All Sky Astrophysics in 3 Dimensions (ASTRO 3D)

Luca Cortese
International Centre for Radio Astronomy Research (ICRAR), University of Western Australia, Crawley, WA 6009, Australia and ARC Centre of Excellence for All Sky Astrophysics in 3 Dimensions (ASTRO 3D), Australia

Feng Yuan
Key Laboratory for Research in Galaxies and Cosmology, Shanghai Astronomical Observatory, Chinese Academy of Sciences, 80 Nandan Road, Shanghai 200030, China

Renbin Yan
Department of Physics and Astronomy, University of Kentucky, 505 Rose Street, Lexington, KY 40506-0055, USA

Chengpeng Zhang
Kavli Institute for Astronomy and Astrophysics, Peking University, 5 Yiheyuan Road, Haidian District, Beijing 100871, P.R.China

Jing Dou
Kavli Institute for Astronomy and Astrophysics, Peking University, 5 Yiheyuan Road, Haidian District, Beijing 100871, P.R.China

Draft version January 3, 2019

ABSTRACT

We study how star formation (SF) is quenched in low-redshift disk galaxies with integral-field spectroscopy. We select 131 face-on spiral galaxies with stellar mass greater than $3 \times 10^{10} M_{\odot}$, and with spatially resolved spectrum from MaNGA DR13. We subdivide the sample into four groups based on the offset of their global specific star formation rate (SFR) from the star-forming main sequence and stack the radial profiles of stellar mass and SFR. By comparing the stacked profiles of quiescent and star-forming disk galaxies, we find that the decrease of the global SFR is caused by the suppression of SF at all radii, but with a more significant drop from the center to the outer regions following an inside-out pattern. As the global specific SFR decreases, the central stellar mass, the fraction of disk galaxies hosting stellar bars, and active galactic nuclei (AGNs; including both LINERs and Seyferts) all increase, indicating dynamical processes and AGN feedback are possible contributors to the inside-out quenching of SF in the local universe. However, if we include only Seyferts, or AGNs with EW(Hα) > 3Å, the increasing trend of AGN fraction with decreasing global sSFR disappears. Therefore, if AGN feedback is contributing to quenching, we suspect that it operates in the low-luminosity AGN mode, as indicated by the increasing large bulge mass of the more passive disk galaxies.

Subject headings: galaxies: evolution — galaxies: star formation — galaxies: active — galaxies:

structure

1. INTRODUCTION

Galaxies in the local universe are clearly separated into two populations in the color-magnitude diagram (CMD), "Red Sequence" and "Blue Cloud," with only few galaxies scattering between forming a "Green Valley (GV)." This bimodality in distribution of galaxy optical properties in terms of their star formation (SF) activity, is found to be not only related with evolutionary stage, but also closely correlated with morphology of a galaxy (e.g., Kauffmann et al. 2003b; Wuyts et al. 2011). Star forming galaxies (SFGs) are dominated by spiral disks, while spheroidal galaxies show little or no emission generated from the H II region ionized by young stars. Any mechanism that changes galaxies into 'red and dead' (i.e., quenching) is required to explain the morphological transformation in a self-consistent way.

What causes the quenching of a galaxy has long been debated. Many factors are proven to be important in suppressing SF but responsible mechanisms are not exactly the same in different galaxies. Following the reddening direction of CMD, the mode of historical SF in galaxies changes from a long-timescale pattern into a major merger triggered starburst (Smethurst et al. 2015), suggesting an evolution in quenching mode from early to late cosmic epoch (Huertas-Company et al. 2016). Theoretical and numerical works require active galactic nuclei (AGNs) feedback in stopping SF to form local massive early-type galaxies (Eisenreich et al. 2017, and references therein), which are quenched ~ 10 Gyr ago (Kauffmann et al. 2003a), with major mergers invoked to explain their rapid star formation history (SFH) and spheroidal morphology (Smethurst et al. 2015). Mergers are also assumed in simulation to form classical bulge in spiral galaxies (Brooks & Christensen 2016, and references therein). However, given the low merger rate in the local universe (Lotz et al. 2011), the build-up of spheroidal structure in the galaxy center could be attributed to other physical reasons rather than mergers. Dynamical processes during secular evolution are considered to be relatively more important in driving (pseudo) bulge formation and passive evolution in present-day galaxies (Gadotti 2011; Kruk et al. 2018, and references therein).

Mass-dependent long-timescale ($\sim$4 Gyr as suggested by Peng et al. 2015) evolution for SFGs is suggested by the finding of the star formation main sequence (SFMS, e.g. Speagle et al. 2014), with the star formation rate (SFR) of most SFGs strongly correlating with their stellar mass following a tight log-linear relation. The flattening in slope of the local SFMS found in the massive end (Lee et al. 2015, e.g.) suggests a mass-related global SF suppression for massive galaxies compared to lower-mass disks, with significant non-starforming bulge/central structure build-up in massive spirals argued to be the most important reason (Abramson et al. 2014; Bluck et al. 2014; Whitaker et al. 2017). Using the position of galaxies on the SFR-M_* diagram with respect to SFMS as a tracer of the current evolutionary stage of galaxies, it have also been found that normal SFGs are almost exponential disks, while starbursts and galaxies fading out of SFMS are observed to be highly concentrated (Wuyts et al. 2011; Guo et al. 2015; Morselli et al. 2017).

"Morphological quenching" is suggested as a morphologically related mechanism that stops SF in massive galaxies, with the existence of prominent bulge increases the Toomre-Q parameter (Toomre 1964), and "stabilizes" gas on disks, i.e., prevents cold gas from collapsing and forming stars (Martig et al. 2009). While this "morphological quenching" naturally leads to an "inside-out" quenching pattern suggested by observation of local massive galaxies (Pan et al. 2015; Belfiore et al. 2018), an alternative inside-out quenching mechanism is also pointed out by observational studies based on mass profiles of galaxies at different evolutionary stages (Tacchella et al. 2015, 2018), with a compaction followed by starburst and gas depletion in galaxy center suggested to be necessary in suppressing SF (Barro et al. 2017; Whitaker et al. 2017). The latter mechanism always requires a dynamical process to trigger gas in the galactic center, to fuel the upcoming intensive central SF and the possible accompanying stellar or AGN feedback.

On the other hand, the finding that galaxies in transition between star forming and quiescent are central low ionization emission-line regions (Belfiore et al. 2017, see also Bär et al. 2017 for AGN hosts above SFMS) directly suggests the feedback of low-luminosity galactic nuclei (LLAGN) as another possible reason of galaxy quenching. However, whether the AGN activity directly correlates with SF intensity or whether the AGN activity is related with the build-up of the central structure in disk galaxies is still not fully understood.

In this paper, we examine the resolved SF properties of massive spiral galaxies crossing the SFMS downward, to statistically explore how stellar mass is assembled during the passive evolution of a galaxy and how does AGN activity relates with the evolutionary stage of SF, aiming to find out if a plausible AGN activity is related with the galaxy structure build-up by comparing the spatial distribution of emission-line ratios with that of SFR and stellar mass (M_*). Obviously there is no direct evolutionary link between current SFGs and quiescent galaxies, with the latter believed to have had active SF in an epoch as early as $z \sim 0.5$ (Peng et al. 2015). However, we can still explore the crucial mechanisms that cause the quenching of a galaxy by comparing present-day galaxies in different evolutionary stages, given that passive galaxies at fixed stellar mass had been sharing the same properties in both morphology and SF activity with SFGs until they faded out of SFMS.

This study is based on the MaNGA (Mapping Nearby Galaxies at Apache Point Observatory, Bundy et al. (2015)) public database from the 13th Data Release of the Sloan Digital Sky Survey (SDSS-DR13; Albareti et al. 2017). Only massive ($M_* > 10^{10.5}$ M$_\odot$) spiral galaxies are examined for the reasons that:
(1) the evolution of massive galaxies is less affected by environmental effects;
(2) quenching and any morphological transformation during quenching events for these galaxies are unlikely to be caused by major mergers.

kxguo@pku.edu.cn, yjpeng@pku.edu.cn

We describe the data analysis in the next section, and show the resolved properties of emission lines and the stellar component in Section §3. We summarize and discuss our results in Section §4. A Chabrier (2003) initial mass function (IMF) is used throughout this work unless otherwise stated. We assume the following cosmological parameters: $\Omega_0 = 0.3, \Omega_\Lambda = 0.7$, and $H_0 = 70\,\mathrm{kms}^{-1}$.

2. SAMPLE AND DATA ANALYSIS

MaNGA is the largest ongoing integral-field unit (IFU) survey of low-redshift galaxies, designed to explore the internal kinematic structure and composition of gas and stars in 10,000 nearby galaxies with a spectral coverage from 3600 to 10300Å at a typical resolution $R \sim 2000$ (Bundy et al. 2015). Galaxies are covered to at least $1.5\,R_\mathrm{e}$ in observation. MaNGA target galaxies are selected from the NASA-Sloan Atlas catalog (NSA; Blanton et al. 2011). The selection has a wide coverage in stellar mass ($M_* > 10^9\,M_\odot$) and optical color, to allow an unbiased analysis of SF of the galaxy population at different evolutionary stages. The median point-spread function (PSF) of the MaNGA data cubes has a median full width at half maximum (FWHM) of $2\farcs5$ (Law et al. 2016), with the standard deviation of $\sim 0\farcs1$ in r-band.

We utilize the visually classified morphology from GalaxyZoo (Lintott et al. 2008, 2011). From 1272 matches found in 1390 galaxies in SDSS-DR13/MaNGA database with a matching radius of 1", 131 spirals with $M_* > 10^{10.5}\mathrm{M}_\odot$ are selected. The stellar masses are taken from the NSA v1_5_4 catalog [1]. We have avoided highly inclined galaxies by removing those with axis ratio $b/a < 0.5$. These galaxies are distributed in the redshift range $0.02 < z < 0.14$, with a median value $z_\mathrm{med} = 0.05$. 118 (90%) galaxies in our sample are distributed within $0.02 < z < 0.08$.

The data cubes of our targets are rebinned to $1'' \times 1''$ pixels, to remove the covariances between neighboring pixels. The rebinning also speeds up the spectral fitting afterward. A map of the signal-to-noise ratio (S/N) calculated in the Hα region (rest-frame $6525 - 6610$Å) is made for each galaxy. Voronoi binning (Cappellari & Copin 2003) is then applied to those pixels with S/Ns less than 30. The covariance in pixel binning is accounted for simply by applying

$$\mathrm{noise_{covar}}/\mathrm{noise_{no\_covar}} = 1 + 1.62 \times \log(\mathrm{N_{bin}}), \quad (1)$$

following the online instructions of MaNGA data reduction[2]. The foreground galactic extinction is estimated based on the dust map of Schlegel et al. (1998), and is corrected using the Galactic extinction law of Cardelli et al. (1989) with $R_V = 3.1$.

The spectral fitting pipeline LZIFU (Ho et al. 2016) is utilized to analyze stellar component and emission lines. Stellar continuum is fit and extracted using the "penalized pixel-fitting" (pPXF) routine (Cappellari & Emsellem 2004; Cappellari 2017), before fitting Gaussian line profiles to emission lines. Weighted simple-stellar-population (SSP) templates from MIUSCAT (Vazdekis et al. 2012) are applied in continuum fitting for the entire wavelength coverage. A Salpeter IMF is used [3]. The stellar mass for each pixel is estimated by summing up the weights of the best-fit stellar templates. Pixels that belong to other sources in the field of view rather than target galaxies have been selected and masked based on segmentation maps reduced from SDSS/r-band images. We then classify the pixels in terms of their position on the Baldwin et al. (1981, BPT) diagram, by comparing their [O III]/Hβ and [N II]/Hα with those of SFGs and AGNs, following Kewley et al. (2006) and adopting the empirical separation between Seyfert and LINER defined by Schawinski et al. (2007). Thus pixels of each galaxy are classified into *Star-forming, Composite, LINER-like* and *Seyfert-like* regions. We refer to Brinchmann et al. (2004) for the classification of pixels with $1 < \mathrm{S/N} < 3$ in any lines. Particularly, we assign pixels which have [N II]/H$\alpha > 0.6$ and $\mathrm{S/N} \geq 3$ in both lines but $\mathrm{S/N} < 3$ in Hβ or [O III] to be LINER-like regions.

3. METHODS AND RESULTS

The position of each galaxy on the integrated SFR- M_* plot (Figure 1) indicates their global evolutionary stage. Galaxies are classified into Starbursts, normal SFGs, GV galaxies and Red Sequence galaxies according to their integrated SFR and their distance to the SFMS at the same stellar mass. To explore the mechanisms that suppress the the global SFR, the resolved properties of the galaxies including stellar mass, SFR, light-weighted stellar age (indicated by Dn4000) and dominated ionization mechanism are analyzed.

3.1. *SF phase classification*

Given the relatively high sample completeness and accuracy in SFR estimation, we use *GALEX*-SDSS-WISE Legacy Catalog (GSWLC-X1, Salim et al. 2016) as the reference catalog to construct SFMS in the redshift range of our MaNGA galaxies. The SFR estimation in this catalog is based on broadband photometry. It has an advantage of being less affected by AGN-heated dust emission, and does not suffer from uncertainties of aperture correction. The SFMS constructed based on the data above [4] is given by:

$$\log(\mathrm{SFR}/(\mathrm{M_\odot yr^{-1}})) = 0.51 \times \log(\mathrm{M_*/M_\odot}) - 5.28 \quad (2)$$

indicated by the blue dotted line in Figure 1. This is determined by a log-linear fit for galaxies with $M_* > 10^{9.4}\,\mathrm{M}_\odot$ which construct a gaussian-like SFR distribution above the separation between SFGs and passive sequence.

We define galaxies with SFRs 0.2 dex above the SFMS as "Starburst" (**SB**) galaxies; galaxies with SFRs between SFMS+0.2 dex and SFMS−0.2 dex as Main Sequence (**MS**) galaxies; galaxies with SFRs between SFMS−0.2 dex and SFMS−0.6 dex as **GV** galaxies; and

[1] We divide the stellar mass in the NSA catalog by a factor of 0.49 to keep the consistency of cosmology.

[2] http://www.sdss.org/dr13/manga/manga-caveats/

[3] SSP spectral energy distributions (SEDs) of metallicity $[\mathrm{Z/H}] = -0.71, -0.40, 0, +0.22$ and age from 63 Myr to 18 Gyr (0.2 dex steps) with unimodal IMF of slope 1.3 (i.e., Salpeter case) are used in continuum fitting. All resolved properties are based on Salpeter IMF to keep the consistency. Later in the text, the integrated Hα-based SFR is corrected to Chabrier IMF to compare with that from the GSWLC-X1 catalog.

[4] To construct the SFMS, we select galaxies in the GSWLC-X1 catalog with the same redshift distribution of galaxies in NSA v1_5_4 catalog.

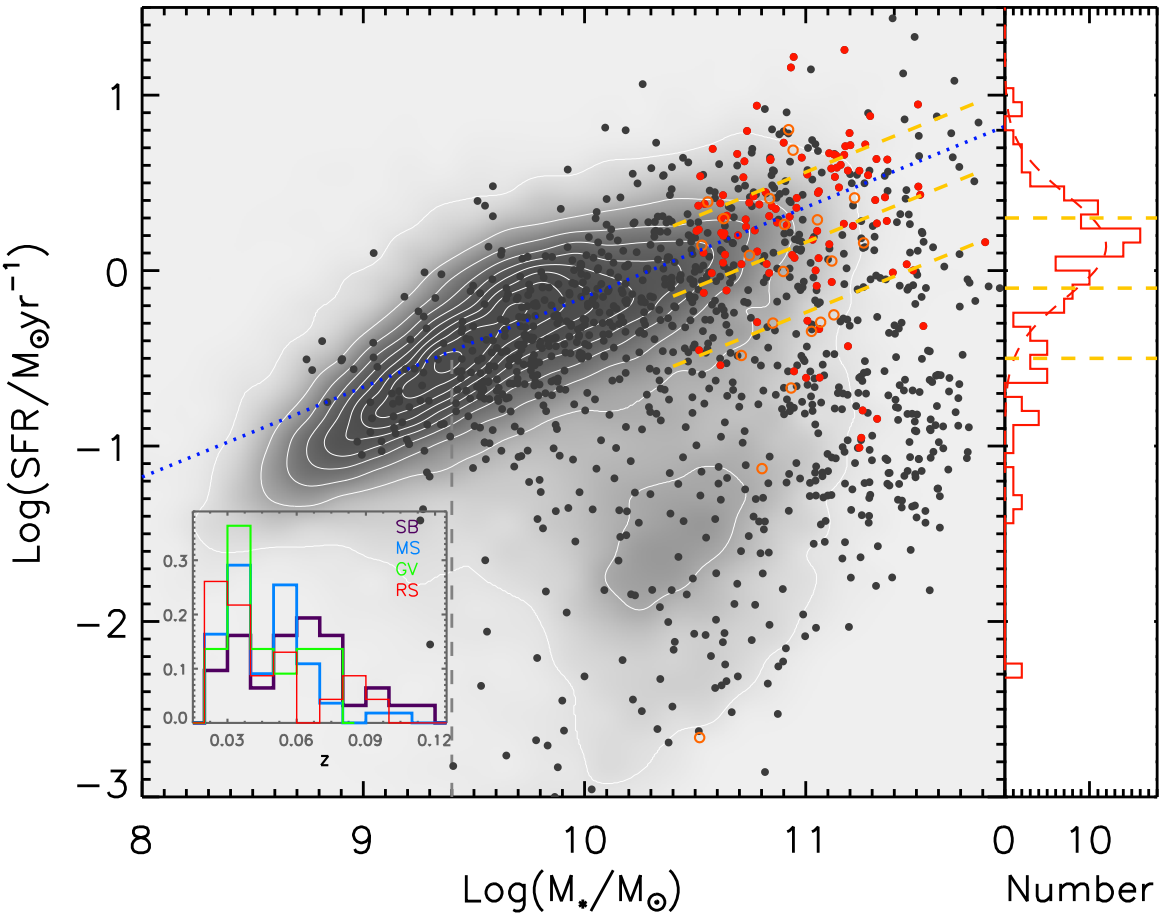

FIG. 1.— Relation between integrated SFR and M_* of SDSS-DR13/MaNGA galaxies (black dots, only galaxies matching GSWLC-X1 are shown). Red dots and orange circles indicate our target face-on spirals with and without GSWLC counterparts, respectively. For the latter, integrated SFR from Hα (see §3.1) is used. The distribution of GSWLC galaxies with the same redshift and stellar mass distribution of SDSS-DR13/MaNGA galaxies is shown by the greyscale background and contours, with the vertical gray dashed line indicating a completeness limit in stellar mass. The right panel shows the SFR distribution of the massive face-on spirals (red+orange) relative to SFMS (blue dotted line), normalized to the corresponding SFR at $\log(M_*/M_\odot) = 10.5$. Yellow dashed lines in either panel show the separations between Starbursts (**SB**s), Main Sequence galaxies (**MS**s), Green Valley galaxies (**GV**s) and Red Spiral galaxies (**RS**s, see §3.1). The lower-left inner panel shows the normalized redshift distribution of galaxies in the four classes.

those with SFRs below SFMS−0.6 dex as passive spiral galaxies (**RS**s). It should be noted that a more conventional definition of **SB** galaxies (**RS** galaxies) would require a higher (lower) cut of SFR relative to the SFMS. This will, however, give too few galaxies classified as SB galaxies and RS galaxies, due to the relatively small size of our sample. Therefore, we adopt the above operational definition of each class.

We cross-match the NSA v1_5_4 catalog with GSWLC-X1 using 1″ as matching radius, [5] and adopt SFRs from GSWLC catalog for the matched sample. Within the selected 131 massive spiral galaxies in our MaNGA sample, 115 of them have matches. For the other 16 galaxies that do not have matches in the GSWLC-X1 catalog, we calculate their SFR by summing up all the dust-corrected Hα emission from star-forming regions defined in §2 using the formula from Kennicutt (1998):

$$\mathrm{SFR} = 7.9 \times 10^{-42} L_{\mathrm{H}\alpha,\mathrm{corr}}, \quad (3)$$

which should be considered as a lower limit for the reason of both ignoring SF from other gas-ionized regions and the limited radial coverage of MaNGA observation. Dust extinction is derived from the observed Blamer decrement with intrinsic Hα/Hβ = 2.86, using Cardelli et al. (1989) extinction law applied with $R_V = 3.1$ and other coefficients updated by O'Donnell (1994). We have compared the SFR from the GSWLC catalog and that from integrated Hα emission for the matched galaxies, which is shown in Figure 2. Because the nontrivial aperture correction is out of the scope of this article and, MaNGA-based SFR is on average smaller than that from GSWLC, we decide to use the latter in classifying the global evolutionary stage of a galaxy. The global Hα-based SFR is divided by a factor of 1.7 to be compared to the Chabrier IMF-derived SFR in GSWLC.

By comparing the position of the 131 face-on massive spirals of our MaNGA galaxy sample with SFMS defined in equation (2) (see Figure 1), 31 galaxies are classified as **SB**s, 55 are **MS**s, 22 are in **GV**s and 23 are **RS**s. Though the SFR measurement based on emission lines could be inconsistent with that derived from broadband photometry, the removal of the 16 galaxies with only MaNGA detection does not affect the average distribution of SF or stellar mass for galaxies in different evolu-

[5] 12 more matches would be found if a 3″ matching radius was used. However, these galaxies are either interacting/diffuse or highly inclined, hence we did not include these galaxies in our final sample.

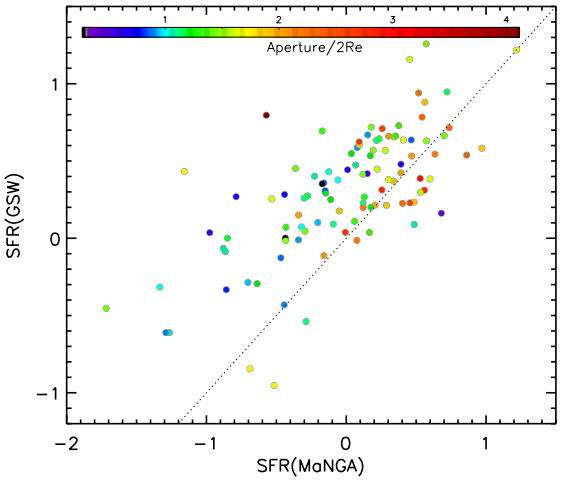

FIG. 2.— The comparison of SFR from *GALEX*-SDSS-WISE Legacy Catalog (GSWLC) with that from integrated Hα emission in all available pixels within an aperture, for the 115 matched galaxies. Different color labels the relative size of an IFU aperture to the half-light radius (''nsa_sersic_th50'') of a galaxy. The dotted line shows a one-to-one relationship. MaNGA-based integrated SFR is on average smaller than that from GSWLC. In general the larger the aperture is, the closer the two measurements are to each other. In this paper we use the GSWLC one to classify the global evolutionary stage of galaxies.

tionary stages. We stress again that **SB**s defined here are those galaxies with integrated SFR 0.2 dex higher than those on SFMS. They do not show any merging features following our visual identification, and could be classified into "Main Sequence" if a more conventional definition of SBs with SFR 4 times higher than the MS galaxies. **RS** is also not necessarily to the same "Red Sequence" as that commonly defined by the literature, which is dominated by fully quenched early-type galaxies about 1 dex below the **MS**. We remind our readers that all these galaxies are "disks" (including those showing clear disks but no distinct spiral arms) in morphology.

3.2. *Stacking and AGN contamination*

To give a clear and global view of the resolved properties of galaxy population in the four different SF phases as defined above, we construct the maps of median M_*, SFR, sSFR, Dn4000 and BPT classification by stacking the galaxies in each SF phase and taking the median values of each stacked pixel, i.e., median stacking. We also construct the one-dimensional (radial) median stacking of SFR, sSFR and M_* which gives a more quantitative way of exploring the evolution in ∼kpc/∼ 0.5 R_e scale.

We ignored the Hα emission from pixels that are not classified as SF regions in calculating global SFR of individual galaxies. However, simply masking out higher-ionized regions leads to an inaccuracy in stacked SFR. This could be either underestimated because of not accounting SF in LINER- or Seyfert like regions, or overestimated by ignoring the un-SF pixels in stacking, due to the low Hα contribution from LINER-like pixels compared to those dominated by H II regions, unless SFR of 0 is assigned to AGN-like pixels and accounted for. Thus we turn to the AGN-SF decomposition method in Kauffmann & Heckman (2009) to refine the SFR from individual pixels according to their position on the BPT diagram. This method offers a statistically reliable estimation of averaged SFR, and the contribution from either side does not suffer from the uncertainty caused by the difference in intrinsic Balmer decrement between AGN-like and H II regions when extinction correction is applied. We apply this method to pixels that are classified as composite, LINER-like, and Seyfert-like in Section §2. The two "pure-AGN" templates based on SDSS spectra used in Kauffmann & Heckman (2009) are adopted. In addition, we adopt a shift of the separation line between SFG and AGN from Kauffmann et al. (2003c) to represent the "Star forming" ridge, so that the SF/composite border is around 50% SF contribution. The classification of "Star forming" and "AGN-like" regions together with the templates used in decomposition are shown in Figure 3.

An S/N cut is applied to pixels before stacking. Since we aim to explore the galaxy properties as a function of distance to galactic center, given that the mass and light distribution of a galaxy generally follows a radially symmetric pattern, we apply a contour binning (Sanders 2006) to pixels with S/N in H$\beta \leq 1$ for each galaxy before extinction correction. A simple deprojection method is also applied to 2D maps of each bin before they are rescaled to physical scales and stacked. In practice, we rotate a galaxy to align its major axis horizontally and elongate the image in the perpendicular direction to match the minor and the major axes, and then we transform the image back to its original size. Since our galaxies are selected to have inclination angles less than 60° ($b/a < 0.5$), the uncertainty caused by the deprojection process does not affect the stacking results. Similarly, with the assumption that disks are circular, radial distance from pixels to galaxy center for individual galaxies are corrected geometrically using their global axis ratio and position angle provided in the NSA catalog.

3.3. *Resolved properties*

Figure 4 shows the median stacked maps of M_*, SFR, SSFR, Dn4000, and the emission-line classification based on the resolved BPT diagram in the panels from the left to the right, for the four populations from **SB** to **RS** indicated by panels from top to bottom. Stacking is only applied to places where the number of available pixels are greater than 3 to make the median estimates reliable. The typical FWHM of PSF is 2.″5, which corresponds to less than 3 kpc, i.e., less than 1 R_e of most galaxies in our sample [6]. Also the redshift distribution of the 4 galaxy groups is identical, as shown in Figure 1 (lower-left panel), the relative difference of resolved properties between different groups without PSF deconvolution should not be affected by the smearing effect. To test this, we have restricted the sample to galaxies with $10^{10.8} < M_*/M_\odot < 10^{11.2}$ in $0.02 < z < 0.08$. The stacked results changed very little.

Figure 4 clearly demonstrates several key features of the resolved properties of the galaxy population, and their changes as the integrated SFR decreases from **SB** (top row) to **RS** (bottom row).

1. As the integrated SFR drops from **SB** to **RS**, a clear increase in the central surface stellar mass

[6] Most (90%) of our galaxies are within the redshift range of $0.02 < z < 0.08$, thus the smearing effect is limited in a scale less than ∼ 3.2 kpc, which is less than 1 R_e for 66% of our sample.

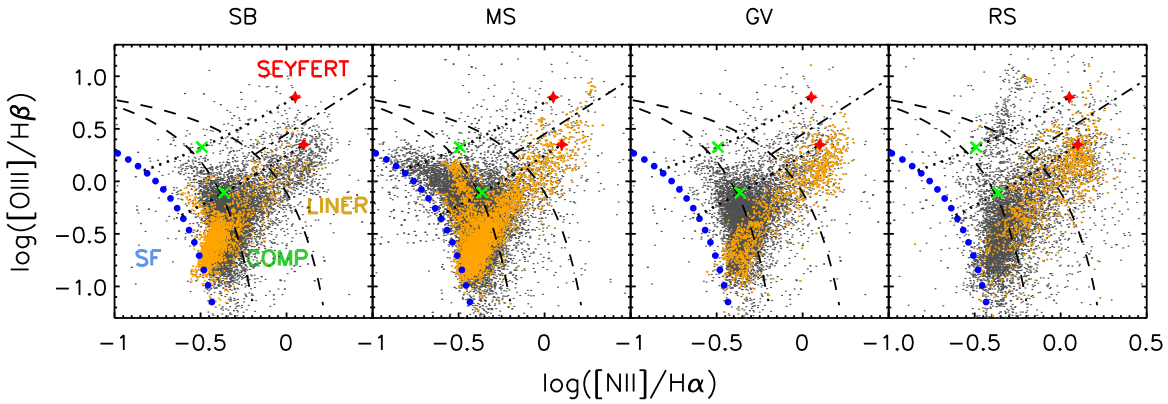

FIG. 3.— The classification of all pixels (black dots) in terms of their position on BPT diagram (log([N II]/Hα) vs. log([O III]/Hβ)), separation between different types utilized by Kewley et al. (2006) and Schawinski et al. (2007) are applied. Pixels within 1 R_e are colored in orange. star-forming, composite, Liner-like and Seyfert-like regions are separated by dashed lines. The two red star symbols in each panel are templates of star-forming galaxies and AGNs adapted from Kauffmann & Heckman (2009), while the blue dotted line is a shift of Kauffmann et al. (2003c) SF/AGN border to make sure the separation between SF and composite to be with 50% SF/AGN contribution. The black dotted lines show two random examples for AGN-SF decomposition described in §3.2, where X symbols indicate the position on the BPT diagram when either side contributes 50% to observed Hα flux. We notice that galaxies, especially the central regions, are dominated by star formation in "Starburst" and "Main Sequence", becoming more composite and LINER-like when they transit to the other two populations.

density is seen. This shows the clear bulge growth during the quenching process.

2. The suppression of SFR in **GV** and **RS** compared to the other two groups is more significant in galaxy center than in the outer disk, with the central-peak in Σ(SFR) distribution disappearing gradually with the passive evolution, resulting in a "ring-like" SF indicated by our stacked **GV** and **RS** disks.

3. The aging of stellar population indicated by Dn4000 and the expanding of which from galaxy center to outer disk are very obvious. This trend goes together with the globally fading of specific star formation rate (sSFR), which shows a significant central-dip pattern since galaxies leave SFMS.

4. The rightmost column shows that disk center appears "LINER-like" in **GV**, and stays like a low-luminosity AGN in **RS** before the galaxy is fully quenched;

We remind our readers that these are all median features. For example, the composite classification for the stacked central region of MS galaxies does not necessarily mean that most of the MS galaxies have a transition-type AGN. Actually only 7 of them have composite centers, while 27/21 in 55 are classified as star-forming/AGN-like.

To give a quantitative comparison on the subgalactic scale, we apply a 1D median stack of the $\Sigma(M_*)$ and the Σ(SFR) profiles along the radial direction with the IDL procedure `regroup.pro`. The 1σ scatter around the median value is shown as the shaded area in Figure 5. Both profiles are normalized to make better comparisons. $\Sigma(M_*)$ profiles are all normalized to an integrated M_* of $10^{10.5} M_\odot$, while Σ(SFR) profiles are normalized to the value of SFR on SFMS for corresponding M_*. Σ(SSFR) profiles are derived from the normalized M_* and SFR profiles. A simple approach has been applied to test the beam smearing effect on the stacked profiles, as follows.

The PSF is assumed to be a Gaussian with an FWHM of 2.″5. Individual $\Sigma(M_*)$ profiles are fitted by a sum of four central peaked half-Gaussian functions with width and amplitude as free parameters [7]. The fitting is required to produce the same total integrated M_* as the total M_* derived from broadband photometry in the NSA catalog. We then subtract the 2.″5-FWHM gaussian profile from the stacked profile and find little difference. We have not done this test to the Σ(SFR), due to the large uncertainty in SFR estimation in the galaxy central regions, especially for **GV** and **RS** galaxies with possible AGN contamination, as shown in the right pannels of Figure 5. However, we do not expect significant change in stacked profiles after PSF deconvolution, since the smearing effect is limited in a scale $\leq 1\,R_e$ for most of our galaxies.

As shown in Figure 5, both $\Sigma(M_*)$ and Σ(SFR) change significantly from **SB** to **RS** at all radii, with the largest change in the central regions(≤2 kpc). The central M_* increases ∼0.4 dex from **SB** to **RS** and most of the increase happens during the transition from **MS** to **GV** phase. The percentage of stellar mass within the central 5 kpc diameter region (vertical dashed line of the top-left panel of Figure 5) of a galaxy increase from 31% and 37% in SB and MS, to 51% and 50% in GV and RS, with standard deviations of 19%, 18%, 19% and 28% in the four groups, respectively. This growth of the central stellar mass as the decrease of the global SFR is related to the central peaked SF of **SB** and **MS** galaxies. While the suppression of the SF happens across the entire disk of the galaxy, from the center to the outer regions, the most significant decrease appears at galaxy center, especially if we set the SFR contribution from "LINER-like" pixels to 0 (indicated by dashed lines). Toward the end of this "inside-out" quenching process, the SF in the central regions has dropped about 1.5 dex, in terms of both Σ(SFR) and Σ(SSFR), leaving some residual star formation in the outer disk regions and forming a ring-like structure, which is clearly shown in 2D SFR and sSFR distribution for **GV** and **RS** in Figure 4.

Our results can be understood as the following key

[7] We found that in practice, 4 Guass is the simplest and best fit when multi Gaussian distributions are used in profile fitting.

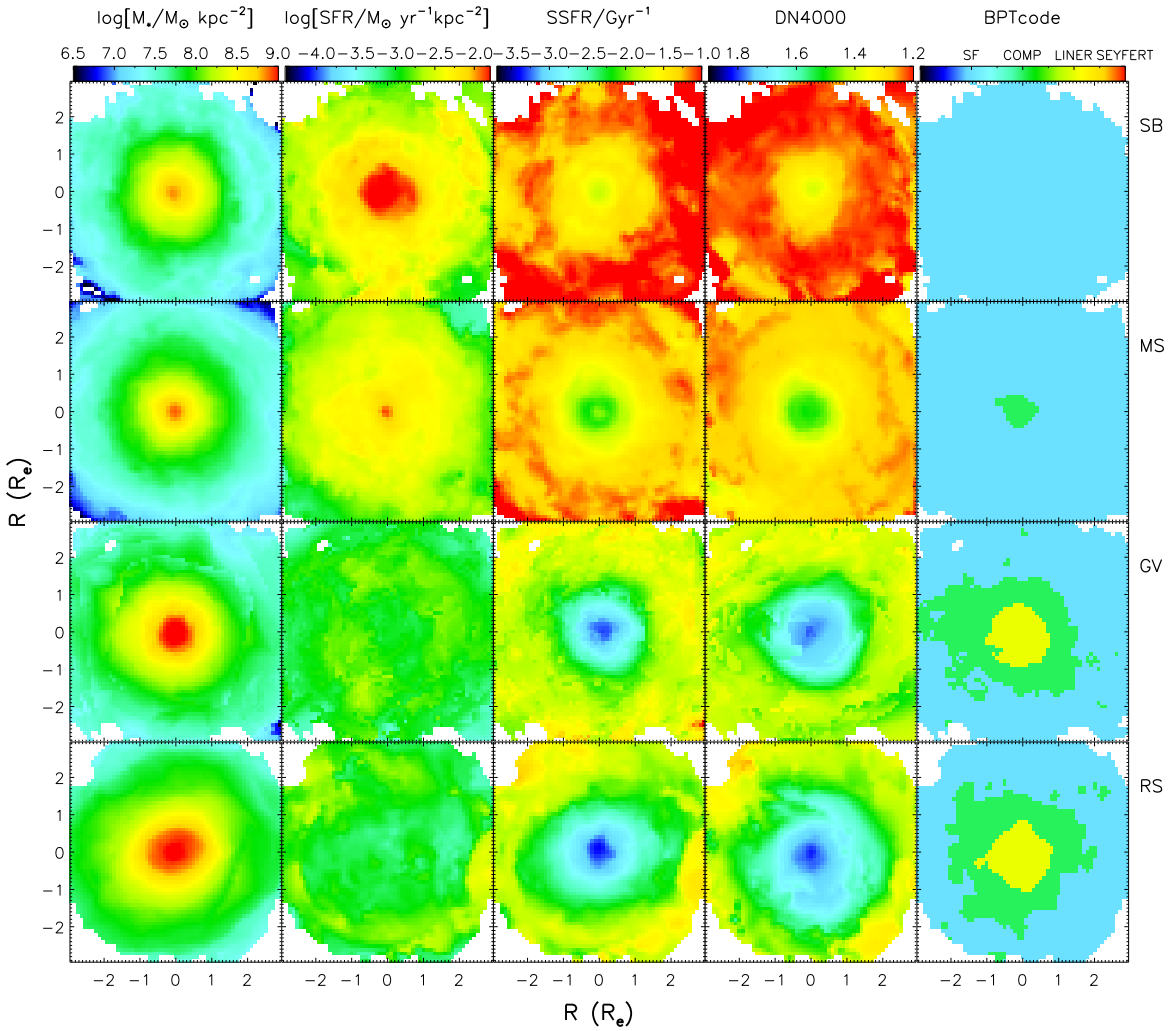

FIG. 4.— Median stacked maps of $M*$,SFR,SSFR,Dn4000, and the position on BPT diagram of each evolution population. Rows from the top down are the stacked maps for **SB, MS, GV** and **RS** respectively. The "BPT code" labeled for the rightmost column is consistent with the color coding of Figure 3, corresponding to populations from star forming region to AGN-like pixels indicated by blue (H II region), green (composite), yellow (LINER-like), and red (Seyfert-like) areas. The total stellar mass of individual galaxies has been normalized to $10^{10.5}M_{\odot}$ to compare the distribution of surface density. SFR here has also been set to the "distance" relative to SFMS as well. It is obvious from this plot that, following the passive sequence indicated by the aging of central stellar population from the top down, star formation in galaxies fades out, the pattern of which transits from a central-peak disk, into a ring-like structure with a dip in galaxy center. It is noticeable that the central part of a galaxy appears "LINER-like" after it falls into **GV** and **RS**.

evolutionary stages for galaxy population:

(1) **SB**s have the youngest stellar population and the most flat stellar disks. Although the SFR profile is peaked in the central regions, the sSFR profile is nearly flat, which indicates the SF is similarly active across the entire disk. Galaxy center shows the strongest emission from the H II region compared to outer parts.

(2) For galaxies on the **MS**, the SF activity becomes lower compared to **SB** galaxies, with a sign of more suppressed SF in the central regions. Accordingly, the dominant stellar population in the galaxy center is getting older as revealed by the Dn4000 map in Figure 4. The emission at galaxy center is still dominated by the H II region.

(3) The dramatic decrease of SF at galaxy center changes the Σ(SFR) profile of a **GV** galaxy into a central-dip function, with a "ring-like" structure appearing at $\sim$5 kpc from galaxy center. Stellar mass, on the other hand, has a prominent build-up in the central area relative to outer disks, which is related to the central-peak SF pattern in **MS** galaxies. The primary emission source at galaxy center is more "LINER-like" rather than SF.

(4) **RS** galaxies show similar mass profiles as those of **GV**s. Both SFR and sSFR profiles continue to decrease from **GV** to **RS**, with a slightly larger decrease in the central regions. The difference almost disappears at $\sim 2R_{\rm e}$, which causes the SFR and sSFR ring-like structure to become more visible in the 2D map as in Figure 4. These galaxies still show "LINER-like" emission, but only limited in 2 kpc from galaxy center in most cases.

Our results are quantitatively consistent with the recent study of Medling et al. (2018) based on SAMI (Sydney-AAO Multi-object Integral-field unit) observa-

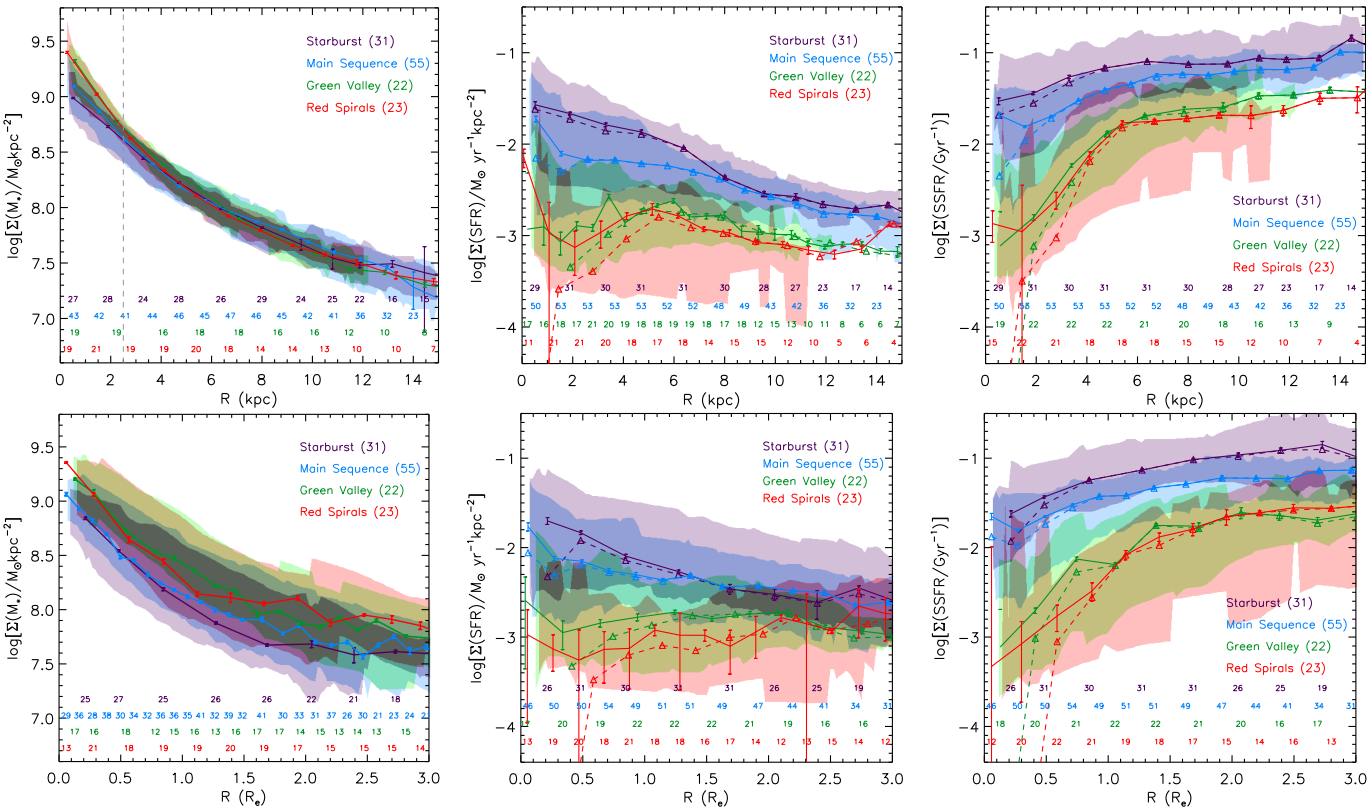

FIG. 5.— From Left to Right panels: Stacked 1D surface density profiles for stellar mass, SFR, and SSFR respectively. Numbers of stacked galaxies in each group are labeled in parentheses. The error bar for each data point is the average combined error of stacked values in each bin. The same normalization as Figure 4 is applied to $\Sigma(M_*)$ and Σ(SFR) before stacking. The top and bottom panels show profiles in units of kiloparsec and R_e respectively. Dashed lines are profiles if we set SFR in composite or AGN-like pixels as 0 before stacking. Shaded areas in each panel indicate the 1σ scatter of the profiles for different groups, limited to radial bins where the numbers of available galaxies (not data points) are greater than 10. The numbers of stacked galaxies in each bin are labeled above the x axis. We estimate the increase of central stellar mass within a 2.5 kpc radius (vertical dashed gray line). The decreasing of SFR is most noticeable in galaxy center compared to the global fading of disks, during the build-up of central stellar mass from **MS** to **RS**.

tions for spiral galaxies in the same Δ(SFMS) and M_* range. Our stacked Σ(SFR) profiles for galaxies from **SB** to **GV** are also consistent with those in Ellison et al. (2018), while the difference between the profiles of red galaxies could have resulted from our different treatments to AGN-like pixels at galaxy center. Again, we need to caution that there is no direct evolutionary link between the four classes from **SB** to **RS**, i.e., the **SB** or the **MS** galaxies are not the progenitors of the **RS** galaxies at the same redshift. A full quenching process is not expected to finish during the redshift range covered by our sample, given a typical quenching timescale of several gigayears. Indeed, the change of the the $\Sigma(M_*)$ profile from **MS** to **GV** cannot be fully explained by integrating the SFR profile over some reasonable quenching timescale. In other words, the change of the $\Sigma(M_*)$ profile from **MS** to **GV** would require a long quenching timescale (> 5 Gyr), or additional mass contribution from mergers or other dynamical processes that can help to increase the $\Sigma(M_*)$. A more comprehensive analysis with consideration of quenching timescale, progenitors at higher redshift, and mergers is necessary and will be discussed in our future work.

4. DISCUSSION AND CONCLUSION

Based on 131 face-on spiral galaxies selected from the SDSS-DR13/MaNGA database, we examine the change of resolved properties of galaxies as the decrease of the global SFR. We find that galaxies slow the speed of SF across their entire disks after they fall out of the SFMS, with a decrease in galaxy center that is much quicker than that in outer disks. Stellar mass also has a quick build-up at galaxy center, with a speed that is 0.4 dex faster than that on disks farther out than $\sim$4 kpc. Galaxy center appears like a LINER host after the SF within the central 2 kpc decreases to $\leq 0.01\,M_\odot\,yr^{-1}$. From then on, a hole in sSFR distribution becomes more significant, with the stellar component at galaxy center dominated by the old population, which continuously expands outward as the global damping of SF. The SFR profile transits from a central-peak function into a "ring-like" central-dip pattern, with a relatively active (but still faint) SF piling up at around $\sim$5 kpc.

Our findings are consistent with the popular "inside-out" mode of quenching for massive galaxies, in which central SF drops faster than outer disks. Combined with the mass build-up in the central 2 kpc before galaxies enter "GV" , our results agree with Fang et al. (2013) in structure-quenching mechanisms (see also Tacchella et al. 2015, 2018), which may be caused by stabilization of gas by the bulge/bar-driven process, during which AGN feedback could also take a part.

To qualify this, we plot the evolution of the fraction of barred galaxies and AGN hosts during the fading of global SF of disks in Figure 6. We adopt a morphology catalog from Galaxy Zoo 2 (Willett et al. 2013) and

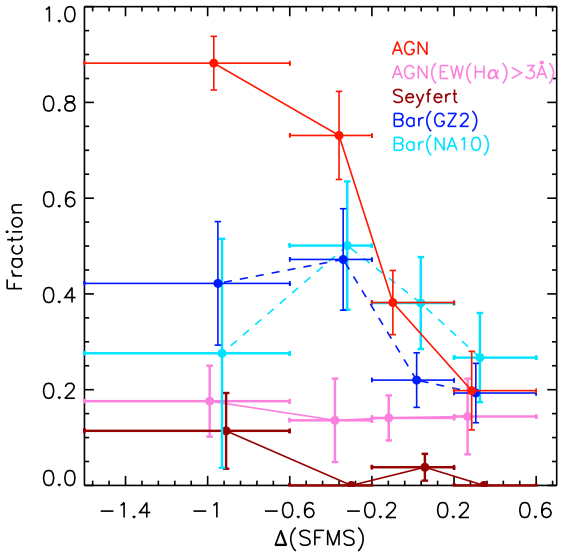

FIG. 6.— Fraction of AGN-host and barred galaxies in a sample of different populations in terms of global star formation stage (from left to right: Red Sequence, Green Valley, Main Sequence, Starburst). Galaxies with their central pixel belong to *LINER-like* or *Seyfert-like* regions in a resolved-BPT diagram of individuals, are classified as AGN hosts. We adopt bar classification from two morphology catalogs, Galaxy Zoo 2 (Willett et al. 2013) and Nair & Abraham (2010), 125 and 72 matches are found respectively. Errors shown in this figure are calculated from the bootstrapping method and the medians of mass are slightly moved for a clear distinction. An increasing fraction of barred galaxies during the fading of star formation is suggestive from this plot (blue and cyan). At the same time, an increase in AGN fraction based on resolved BPT diagram is also clearly shown (red). However, this trend almost disappears when only Seyfert galaxies (dark red) or those with central EW(Hα) > 3Å (pink) are considered.

Nair & Abraham (2010) to classify barred galaxies in our sample. Differences between the classification are mainly due to the deviation in sample coverage of these catalogs. AGN hosts are galaxies with their central pixels classified as "LINER-" or "Seyfert-like" in resolved BPT diagrams (see Figure 4) [8]. The increase of AGN fraction during the passive evolution is clearly seen from Figure 6. A significant increase in bar fraction after galaxies leave MS and fade into GV is also indicated [9].

4.1. *Dynamical processes in inside-out quenching*

As our target galaxies are massive spirals that are not supposed to have experienced significant disruption in structure triggered by, e.g., major mergers, secular evolution is an important mechanism for galaxy evolution and quenching. Bars are suggested to play a central role in building the dense central component, by driving gas inflow to trigger SF in galaxy center (Kormendy & Kennicutt 2004; Lin et al. 2017). After the in-falling gas has all been consumed by stars, a strong bar "sweeps" out star forming resources or increases the gas random motions within the corotation radius (Khoperskov et al. 2018; Spinoso et al. 2017), leaving an "star formation desert" within the central ∼2 kpc (James, & Percival 2018).

Compared with ∼ 20% and ∼ 22% bar galaxies found in **SB** and **MS**, half of our spirals in **GV** and **RS** are identified as barred galaxies in Galaxy Zoo 2 (Willett et al. 2013) and Nair & Abraham (2010). The increase of the bar percentage with the decrease of both global and inner-several-kiloparsec SF, which is most prominent between MS and GV, agrees with the "bar-quenching" mode suggested in massive galaxies from both observation and simulation (Gavazzi et al. 2015; Haywood et al. 2016; Kruk et al. 2018, see also Kim et al. 2017). Additionally, almost all of the last half central-red galaxies are inner lens/oval galaxies. From a scenario in which bars dissolve into lenses(Heller et al. 2007), the quenching of the central SF in these galaxies could also be driven by bars. However, we did not find a significant enhancement of central SF caused by bar-triggered gas inflow before the suppression, in barred galaxies of **SB** and **MS** compared to those unbarred, which is observed in Kim et al. (2017) and Catalán-Torrecilla et al. (2017). This may be caused by our limited barred sample (6 found in **SB** and 12 found in **MS**). Bar strength could be another reason because there is barely any difference found between weakly barred and unbarred galaxies (Kim et al. 2017).

The anticorrelation between the SF activity and bar fraction shown in Figure 6 is also consistent with theoretical studies in which bar formation is argued to be suppressed or delayed in gas-rich disks(e.g., Athanassoula et al. 2013), implying a possible relation between bar size/strength with on-going SF or optical color, as pointed out by Erwin (2018). Similarly in observation, Cervantes Sodi (2017) has found an anticorrelation between HI gas richness and bar fraction, agreeing with studies in which bars are more frequently found in massive and red early-type galaxies (e.g, Erwin 2005; Nair & Abraham 2010; Lee et al. 2012). On the other hand, bars can also take a part in fueling gas into the galactic center and can trigger an enhancement of SF in situ (e.g. Berentzen et al. 2007). The lack of discovery of the high fraction of strong bar for SB/starbursts, which however was shown by Wang et al. (2012), could result from the deviation in bar identification between studies. Given that the bar strength in Wang et al. (2012) is parameterized in terms of ellipticity, the contradiction could also be due to a potential dependence of bar ellipticity on central stellar mass, which is a natural result of the inverse correlation between bar ellipticity and central dynamical mass concentration found by Das et al. (2003) based on CO observation.

The finding of a ring in SFR distribution between around 4-6 kpc ($\sim 2\,R_e$) is noticeable in the last two stages of global SF. This wide range shown in stacked 1D and 2D profiles resulted mostly from the scatter in galactic size. While a bar triggering suppression of the central SF naturally lead to a ring-like SF in the outer part of a galaxy, a combination of AGN feedback and bar-driven gas inflow also triggers an enhancement of SF and forming a dense ring at a finite radius (Robichaud et al. 2017). As Robichaud et al. (2017) address, this scenario is rather a "displacement" than a "suppression" of SF, because the gas is pushed to outer radii instead of thermalized or consumed.

A related high-redshift work (Genzel et al. 2014) that

[8] Although composite objects could also be powered by AGNs, their numbers are small (3, 7, 1, and 0 in four groups, respectively) compared to either star-forming or AGN-like galaxies, and could be counted into statistical errors in AGN fraction.

[9] The increase in the bar fraction from SFGs to quiescent galaxies is more prominent if we constrain the sample to galaxies with $M_* \leq 10^{11}\mathrm{M}_\odot$, which is from 0.11 for SB and 0.12 for MS, to 0.50 for GV and 0.43 for RS.

also found a Hα ring argued for a different inside-out quenching mechanism for massive SFGs, where a centrally peaked Toomre-Q distribution caused by the higher concentration of stellar mass prevents further SF in galaxy center. This "gravitational quenching" or "Morphological quenching" (Martig et al. 2009) has been highlighted in explaining the formation of red galaxies with quenched gas disks. And SF is confirmed less efficient in bulge-dominated galaxies than in pure disks from both HI and H_2 observation (e.g., Kennicutt 1989; Saintonge et al. 2012). However, compared to the consistency in the effect of the bulge-related mechanism argued among the literature, the role that bar leads in quenching is still concealed. A further analysis with a more complete sample of the dynamics and the gas contents of barred galaxies is required to test the scenarios.

The passive evolution of disks as shown in our work is related to but not exactly the "compaction" suggested for quenching of high-redshift galaxies (Dekel et al. 2009; Zolotov et al. 2015, and reference therein). Similar mechanisms require galaxies that are still on the main sequence experiencing a starburst to induce gas depletion and quenching afterward, which is also suggested in recent work by Ellison et al. (2018) based on their analysis of the gas-phase metallicity profile. Though **SB** is more metal-poor gas rich at galaxy center, our finding of the higher $\Sigma(M_*)$ in the center of **MS** than **SB** galaxies shows that starbursts may not be powerful enough to cause a compaction, either to deplete gas in galaxy center or to quench SF. However, we should restate that compared to those extremes, which form most of stars in very short timescales, our **SB**s are more likely normal SFGs scattering above SFMS further than normal SFGs. Additionally, accounting for the relatively short timescale of "compaction", the $\Sigma(M_*)$ profile for **SB** and **MS** galaxies plausibly do not show significant difference. Nevertheless, the faster mass growth in galaxy center compared to that in the outer disk for fixed M_* certainly indicate a shrink in galaxy size (effective radius), which could also be caused by dynamical reasons like bar-driven processes other than SF only. A more detailed self-consistent analysis with a proper assumption in SFH is required for further studies.

4.2. *The puzzling role of AGNs in quenching SF*

Only 10 in 117 of our galaxies are classified as AGNs in the MPA-JHU catalog (Tremonti et al. 2004) based on the SDSS spectrum, including 1 **SB**, 5 **MS**s, 3 **GV**s and 1 **RS** galaxies. However, from resolved analysis, 16 of 22 **GV**s and 20 in 23 **RS** galaxies show AGN-like emission in their central regions, and 34 of them in total could be classified as LINERs. Compared with the HII dominated "Starburst" and "Main Sequence," this finding of the LINER-dominated other two groups qualitatively agree with the recently suggested "LI(N)ER" sequence of Hsieh et al. (2017). These galaxies are either classified as Type-2 AGN hosts (Catalán-Torrecilla et al. 2017) or "cLIER"s (Belfiore et al. 2017) in related studies. However, because of their old underlying stellar population, and relatively extended spatial distribution, instead of low-luminosity activity nuclei, the emission sources of the harder ionization field compared to the HII region are suspected to be low-mass hot evolved stars (e.g., Binette et al. 1994; Sarzi et al. 2010; Cid Fernandes et al. 2011; Yan & Blanton 2012; Papaderos et al. 2013; Singh et al. 2013).

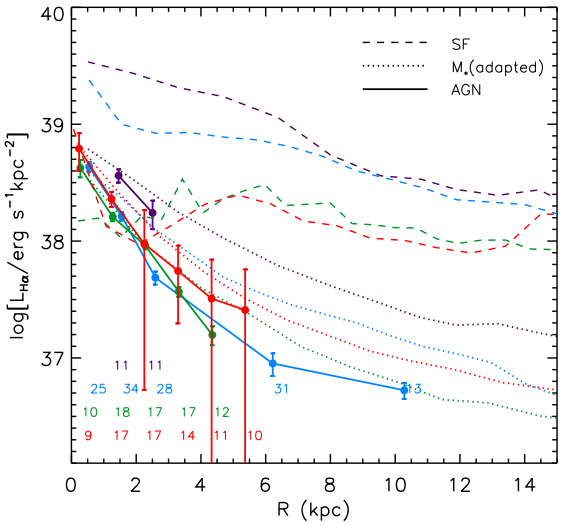

FIG. 7.— Median Hα profiles of AGNs (solid lines) in comparison with that from star formation (dashed lines). $\Sigma(M_*)$ profiles are also shown as dotted lines with adaptive normalizations to be compared with the Hα profiles. The color coding is the same as that in Figure 5. Only bins in which the number of galaxies stacked is not less than nine are shown. Numbers in each bin are indicated above the x axis. Hα emission from AGNs is based on the AGN-SF decomposition described in §3.2. Dust attenuation is corrected with the assumption of intrinsic Hα/Hβ = 3.06 (Dong et al. 2008). A central-peak pattern in AGN emission is clearly shown.

A mixture of low-luminosity AGN and old stellar component indeed could not be ruled out in red galaxies. The universality of the "LINER-like" emission we find in the SF suppressed disk center agrees with the concentrated distribution of the old stellar population in red galaxies, the emission from which is overshined by SF before a galaxy drops off the SFMS, preventing itself from being distinguishable until young and massive stars fade away. On the other hand, given the gently decreasing $\Sigma(M_*)$ profile from center to outside in each population, the point-source-like central-peak pattern of the Hα profile contributed from pure "AGNs" (from the empirical AGN/SF decomposition) as shown in Figure 7 implies a plausible existence of "real" LINER emission within the central 2 kpc, and could hardly be explained by an excess of the population of hot evolved stars at galaxy center (also see the discussion in §6.3 of Ho 2008).

A quick check of individual 2D EW(Hα) maps reveals that around one-fifth of our "cLIERs" should be true AGNs from their emission in central pixels [10] based on the criteria suggested by Cid Fernandes et al. (2011). However, the increasing pattern of the AGN fraction disappears if we throw out the "retired galaxies" defined above or if only Seyferts are considered (Figure 6). Thus despite the plausible contribution of AGNs to the steep Hα profiles, the concentrated Hα emission in **GV** and **RS** could also partly be seen as a combined result of the depression in central HII emission (dashed line in Figure 5) and the centrally concentrated distribution of stellar mass, i.e., an outcome of the competition between young and old populations. In this case, the concen-

[10] The result does not change within 1σ if we calculate the integrated EW(Hα) within a R_e or 2.3kpc (corresponding to 1" in $z \sim 0.13$) instead.

trated old population at galaxy center, i.e., bulge, could play a more important role than AGNs in triggering the quenching of an SFG, given that most stellar mass at galaxy center has already been formed before a galaxy become **GV**. This process is related to the "morphological quenching" (Martig et al. 2009) or "gravitational quenching" (Genzel et al. 2014) discussed in the last subsection. Nevertheless, given the well-known correlation between the mass of the black hole and that of bulge, a **GV** or **RS** galaxy that has already built up its compact central component should undoubtedly contain a massive black hole. Moreover, because 85% (57 in 66) of nearby LINER host galaxies were found to have X-ray cores in a recent study (She et al. 2017), we cannot rule out the effect of AGN feedback on SF given our high fraction of LINER hosts in nearly quenched spirals.

Indeed, besides the processes caused by central stellar bulge or bar, our findings also agree with AGN-driven quenching in state-of-the-art simulations. Given the high fraction of "LINER-like" host galaxies in contrast to the rare "Seyfert" hosts (Figure 6), LLAGN could take a more important role in affecting global SF in galaxies. The low-accretion-rate mode is found to dominate the duty cycle of an AGN (e.g., Ho 2008), suggesting an important cumulative effect of the corresponding "hot-mode feedback" (Yuan et al. 2018) on SF. Both energy and momentum are injected into the surrounding interstellar medium, thermalizing, and/or diluting the materials for further SF.

Wind emitted from AGNs is found to play a more important role in quenching galaxy disks than radiation (Figure 8 in Yuan et al. 2018, see also Weinberger et al. 2017, 2018). Our finding of the suppression of SF in the central 2 kpc region in LINER hosts is likely because of the kinetic wind launched by the hot accretion flow (Yuan et al. 2015) in the "hot feedback mode." [11] Although there could be other mechanisms depleting cold gas and preventing gas inflow when gas supply is still plentiful at galaxy center, our results suggest a possible quenching mechanism of low-luminosity AGN feedback, if the emission source of "LINER" could be confirmed as a real AGN.

We thank the anonymous referee for their valuable comments and suggestions that helped to improve the manuscript. We thank the discussions with Prof. Jing Wang, Prof. Martin Bureau, Prof. Michele Cappellari, Prof. Chris Lintott, and Dr. Zhi-zheng Pan. The first author is grateful for the constant encouragement of Prof. Xian-zhong Zheng. Y.P. acknowledges support from the National Key Program for Science and Technology Research and Development under grant No. 2016YFA0400702, and the NSFC grant No. 11773001. H.F. acknowledges support from the National Science Foundation under grant AST-1614326. Parts of this research were conducted by the Australian Research Council Centre of Excellence for All Sky Astrophysics in 3 Dimensions (ASTRO 3D), through project number CE170100013. This research is also supported jointly by China National Postdoctoral Science Foundation, China Scholarship Council and The International Centre for Radio Astronomy Research.

Funding for the Sloan Digital Sky Survey IV has been provided by the Alfred P. Sloan Foundation, the U.S. Department of Energy Office of Science, and the Participating Institutions. SDSS-IV acknowledges support and resources from the Center for High-Performance Computing at the University of Utah. The SDSS website is www.sdss.org.

SDSS-IV is managed by the Astrophysical Research Consortium for the Participating Institutions of the SDSS Collaboration including the Brazilian Participation Group, the Carnegie Institution for Science, Carnegie Mellon University, the Chilean Participation Group, the French Participation Group, Harvard-Smithsonian Center for Astrophysics, Instituto de Astrofísica de Canarias, The Johns Hopkins University, Kavli Institute for the Physics and Mathematics of the Universe (IPMU) / University of Tokyo, Lawrence Berkeley National Laboratory, Leibniz Institut für Astrophysik Potsdam (AIP), Max-Planck-Institut für Astronomie (MPIA Heidelberg), Max-Planck-Institut für Astrophysik (MPA Garching), Max-Planck-Institut für Extraterrestrische Physik (MPE), National Astronomical Observatories of China, New Mexico State University, New York University, University of Notre Dame, Observatário Nacional / MCTI, The Ohio State University, Pennsylvania State University, Shanghai Astronomical Observatory, United Kingdom Participation Group, Universidad Nacional Autónoma de México, University of Arizona, University of Colorado Boulder, University of Oxford, University of Portsmouth, University of Utah, University of Virginia, University of Washington, University of Wisconsin, Vanderbilt University, and Yale University.

REFERENCES

Abramson, L. E., Kelson, D. D., Dressler, A., et al. 2014, ApJ, 785, L36
Aihara, H., Allende Prieto, C., An, D., et al. 2011, ApJS, 193, 29
Albareti, F. D., Allende Prieto, C., Almeida, A., et al. 2017, ApJS, 233, 25
Athanassoula, E., Machado, R. E. G., & Rodionov, S. A. 2013, MNRAS, 429, 1949
Baldwin, J. A., Phillips, M. M., & Terlevich, R. 1981, PASP, 93, 5
Bär, R. E., Weigel, A. K., Sartori, L. F., et al. 2017, MNRAS, 466, 2879
Barro, G., Faber, S. M., Koo, D. C., et al. 2017, ApJ, 840, 47.
Belfiore, F., Maiolino, R., Maraston, C., et al. 2017, MNRAS, 466, 2570
Belfiore, F., Maiolino, R., Bundy, K., et al. 2018, MNRAS, 477, 3014.
Berentzen, I., Shlosman, I., Martinez-Valpuesta, I., & Heller, C. H. 2007, ApJ, 666, 189
Binette, L., Magris, C. G., Stasińska, G., & Bruzual, A. G. 1994, A&A, 292, 13
Blanton, M. R., Kazin, E., Muna, D., Weaver, B. A., & Price-Whelan, A. 2011, AJ, 142, 31
Bluck, A. F. L., Mendel, J. T., Ellison, S. L., et al. 2014, MNRAS, 441, 599
Brinchmann, J., Charlot, S., White, S. D. M., et al. 2004, MNRAS, 351, 1151
Brooks, A., & Christensen, C. 2016, Galactic Bulges, 418, 317
Bundy, K., Bershady, M. A., Law, D. R., et al. 2015, ApJ, 798, 7

[11] The Σ(SFR) peak we found for green and red galaxies within the central 1 kpc of a disk is also predictable in quenching models of Weinberger et al. (2017) for a galaxy with central-peak gas distribution.

Cardelli, J. A., Clayton, G. C., & Mathis, J. S. 1989, ApJ, 345, 245
Cappellari, M. 2017, MNRAS, 466, 798
Cappellari, M., & Copin, Y. 2003, MNRAS, 342, 345
Cappellari, M., & Emsellem, E. 2004, PASP, 116, 138
Catalán-Torrecilla, C., Gil de Paz, A., Castillo-Morales, A., et al. 2017, ApJ, 848, 87
Cervantes Sodi, B. 2017, ApJ, 835, 80
Chabrier, G. 2003, PASP, 115, 763
Cid Fernandes, R., Stasińska, G., Mateus, A., & Vale Asari, N. 2011, MNRAS, 413, 1687
Cid Fernandes, R., Stasińska, G., Vale Asari, N., et al. 2010, Co-Evolution of Central Black Holes and Galaxies, 267, 65
Das, M., Teuben, P. J., Vogel, S. N., et al. 2003, ApJ, 582, 190
Dekel, A., Birnboim, Y., Engel, G., et al. 2009, Nature, 457, 451
Dong, X., Wang, T., Wang, J., et al. 2008, MNRAS, 383, 581
Eisenreich, M., Naab, T., Choi, E., Ostriker, J. P., & Emsellem, E. 2017, MNRAS, 468, 751
Ellison, S. L., Sánchez, S. F., Ibarra-Medel, H., et al. 2018, MNRAS, 474, 2039
Erwin, P. 2005, MNRAS, 364, 283
Erwin, P. 2018, MNRAS, 474, 5372
Fang, J. J., Faber, S. M., Koo, D. C., & Dekel, A. 2013, ApJ, 776, 63
Fu, H., Steffen, J. L., Gross, A. C., et al. 2018, ApJ, 856, 93
Gadotti, D. A. 2011, MNRAS, 415, 3308
Gavazzi, G., Consolandi, G., Dotti, M., et al. 2015, A&A, 580, A116
Genzel, R., Förster Schreiber, N. M., Lang, P., et al. 2014, ApJ, 785, 75
Guo, K., Zheng, X. Z., Wang, T., & Fu, H. 2015, ApJ, 808, L49
Haywood, M., Lehnert, M. D., Di Matteo, P., et al. 2016, A&A, 589, A66
Heller, C. H., Shlosman, I., & Athanassoula, E. 2007, ApJ, 671, 226
Ho, L. C. 2008, ARA&A, 46, 475
Ho, I.-T., Medling, A. M., Groves, B., et al. 2016, Ap&SS, 361, 280
Hsieh, B. C., Lin, L., Lin, J. H., et al. 2017, ApJ, 851, L24
Huertas-Company, M., Bernardi, M., Pérez-González, P. G., et al. 2016, MNRAS, 462, 4495
James, P. A., & Percival, S. M. 2018, MNRAS, 474, 3101.
Kauffmann, G., & Heckman, T. M. 2009, MNRAS, 397, 135
Kauffmann, G., Heckman, T. M., Tremonti, C., et al. 2003, MNRAS, 346, 1055
Kauffmann, G., Heckman, T. M., White, S. D. M., et al. 2003, MNRAS, 341, 33
Kauffmann, G., Heckman, T. M., White, S. D. M., et al. 2003, MNRAS, 341, 54
Kennicutt, R. C., Jr. 1989, ApJ, 344, 685
Kennicutt, R. C., Jr. 1998, ARA&A, 36, 189
Kewley, L. J., Dopita, M. A., Sutherland, R. S., Heisler, C. A., & Trevena, J. 2001, ApJ, 556, 121
Kewley, L. J., Groves, B., Kauffmann, G., & Heckman, T. 2006, MNRAS, 372, 961
Khoperskov, S., Haywood, M., Di Matteo, P., et al. 2018, A&A, 609, A60.
Kim, E., Hwang, H. S., Chung, H., et al. 2017, ApJ, 845, 93
Kormendy, J., & Kennicutt, R. C., Jr. 2004, ARA&A, 42, 603
Kruk, S. J., Lintott, C. J., Bamford, S. P., et al. 2018, MNRAS, 473, 4731
Law, D. R., Cherinka, B., Yan, R., et al. 2016, AJ, 152, 83
Lee, G.-H., Park, C., Lee, M. G., & Choi, Y.-Y. 2012, ApJ, 745, 125
Lee, N., Sanders, D. B., Casey, C. M., et al. 2015, ApJ, 801, 80
Lilly, S. J., & Carollo, C. M. 2016, ApJ, 833, 1
Lin, L., Li, C., He, Y., Xiao, T., & Wang, E. 2017, ApJ, 838, 105
Lintott, C., Schawinski, K., Bamford, S., et al. 2011, MNRAS, 410, 166
Lintott, C. J., Schawinski, K., Slosar, A., et al. 2008, MNRAS, 389, 1179
Lotz, J. M., Jonsson, P., Cox, T. J., et al. 2011, ApJ, 742, 103
Medling, A. M., Cortese, L., Croom, S. M., et al. 2018, MNRAS, 475, 5194
Morselli, L., Popesso, P., Erfanianfar, G., & Concas, A. 2017, A&A, 597, A97
Martig, M., Bournaud, F., Teyssier, R., & Dekel, A. 2009, ApJ, 707, 250
Nair, P. B., & Abraham, R. G. 2010, ApJS, 186, 427
O'Donnell, J. E. 1994, ApJ, 422, 158
Pan, Z., Li, J., Lin, W., et al. 2015, ApJ, 804, L42
Papaderos, P., Gomes, J. M., Vílchez, J. M., et al. 2013, A&A, 555, L1
Peng, Y.-j., Lilly, S. J., Kovač, K., et al. 2010, ApJ, 721, 193
Peng, Y., Maiolino, R., & Cochrane, R. 2015, Nature, 521, 192
Robichaud, F., Williamson, D., Martel, H., Kawata, D., & Ellison, S. L. 2017, MNRAS, 469, 3722
Salim, S., Lee, J. C., Janowiecki, S., et al. 2016, ApJS, 227, 2
Saintonge, A., Tacconi, L. J., Fabello, S., et al. 2012, ApJ, 758, 73
Sanders, J. S. 2006, MNRAS, 371, 829
Sarzi, M., Shields, J. C., Schawinski, K., et al. 2010, MNRAS, 402, 2187
Schawinski, K., Thomas, D., Sarzi, M., et al. 2007, MNRAS, 382, 1415
Schlegel, D. J., Finkbeiner, D. P., & Davis, M. 1998, ApJ, 500, 525
She, R., Ho, L. C., & Feng, H. 2017, ApJ, 842, 131
Singh, R., van de Ven, G., Jahnke, K., et al. 2013, A&A, 558, A43
Smethurst, R. J., Lintott, C. J., Simmons, B. D., et al. 2015, MNRAS, 450, 435
Speagle, J. S., Steinhardt, C. L., Capak, P. L., & Silverman, J. D. 2014, ApJS, 214, 15
Spinoso, D., Bonoli, S., Dotti, M., et al. 2017, MNRAS, 465, 3729
Tacchella, S., Carollo, C. M., Renzini, A., et al. 2015, Science, 348, 314
Tacchella, S., Carollo, C. M., Förster Schreiber, N. M., et al. 2018, ApJ, 859, 56.
Toomre, A. 1964, ApJ, 139, 1217
Tremonti, C. A., Heckman, T. M., Kauffmann, G., et al. 2004, ApJ, 613, 898
Vazdekis, A., Ricciardelli, E., Cenarro, A. J., et al. 2012, MNRAS, 424, 157
Wang, J., Kauffmann, G., Overzier, R., et al. 2012, MNRAS, 423, 3486
Weinberger, R., Springel, V., Hernquist, L., et al. 2017, MNRAS, 465, 3291
Weinberger, R., Springel, V., Pakmor, R., et al. 2018, MNRAS, 479, 4056.
Whitaker, K. E., Bezanson, R., van Dokkum, P. G., et al. 2017, ApJ, 838, 19
Willett, K. W., Lintott, C. J., Bamford, S. P., et al. 2013, MNRAS, 435, 2835
Wuyts, S., Förster Schreiber, N. M., van der Wel, A., et al. 2011, ApJ, 742, 96
Yan, R., & Blanton, M. R. 2012, ApJ, 747, 61
Yuan, F., Gan, Z., Narayan, R., et al. 2015, ApJ, 804, 101
Yuan, F., Yoon, D., Li, Y.-P., et al. 2018, ApJ, 857, 121
Zolotov, A., Dekel, A., Mandelker, N., et al. 2015, MNRAS, 450, 2327